NANO LETTERS

2009
Vol. 9, No. 8
2855-2861

High-Strength Composite Fibers: Realizing True Potential of Carbon Nanotubes in Polymer Matrix through Continuous Reticulate Architecture and Molecular Level Couplings

Wenjun Ma,[†,#] Luqi Liu,[‡] Zhong Zhang,[*,‡] Rong Yang,[||,#] Gang Liu,[⊥] Taihua Zhang,[||] Xuefeng An,[⊥] Xiaosu Yi,[⊥] Yan Ren,[†,#] Zhiqiang Niu,[†,#] Jinzhu Li,[†,#] Haibo Dong,[†,#] Weiya Zhou,[†] Pulickel M. Ajayan,[§] and Sishen Xie[*,†]

Beijing National Laboratory of Condensed Matter, Institute of Physics, Chinese Academy of Sciences, Beijing 100190, People's Republic of China, National Center for Nanoscience and Nanotechnology, Beijing 100190, People's Republic of China, Department of Mechanical Engineering and Materials Science, Rice University, 6100 Main Street, Houston, Texas 77005, State Key Laboratory of Nonlinear Mechanics (LNM), Institute of Mechanics, Chinese Academy of Sciences, Beijing 100190, People's Republic of China, National Key Laboratory of Advanced Composites, Beijing Institute of Aeronautical Materials, Beijing 100095, China, and Graduate School of the Chinese Academy of Sciences, Beijing 100080, People's Republic of China

Received April 1, 2009; Revised Manuscript Received June 16, 2009

ABSTRACT

Carbon nanotubes have unprecedented mechanical properties as defect-free nanoscale building blocks, but their potential has not been fully realized in composite materials due to weakness at the interfaces. Here we demonstrate that through load-transfer-favored three-dimensional architecture and molecular level couplings with polymer chains, true potential of CNTs can be realized in composites as initially envisioned. Composite fibers with reticulate nanotube architectures show order of magnitude improvement in strength compared to randomly dispersed short CNT reinforced composites reported before. The molecular level couplings between nanotubes and polymer chains results in drastic differences in the properties of thermoset and thermoplastic composite fibers, which indicate that conventional macroscopic composite theory fails to explain the overall hybrid behavior at nanoscale.

To build composites with superior strength and flaw-tolerance, nanoscale reinforcements have natural advantages than their micrometer-sized counterparts because of their paucity of structural defects and high aspect ratio.[1] However, a huge challenge still lies in the manufacturing of a high-performance nanocomposite because of the agglomeration tendency of the nanometer-sized fillers and poor load transfer efficiency between the matrix and reinforcements. A good example is carbon nanotube (CNT) reinforced composites. Although individual CNTs have Young's modulus of 1 TPa and strength over 60 GPa,[2,3] to date CNT reinforced polymer composites fabricated by mixing polymers and nanotubes have shown only moderate enhancement in modulus and even more limited improvements in strength.[4] Even in the cases where CNTs are optimally dispersed at high volume fraction, their moduli and strengths are at least 2 orders of magnitude lower than what was theoretically predicted by composite theory.[5−7]

Essentially, the mechanical performance of CNT reinforced composites relies on the load-bearing status of the CNTs in the matrix. However, two inherent problems of CNTs shadow their promise as efficient load-bearers. One is their waviness. A multiwalled carbon nanotube with a diameter of 10 nm is 10^{12} times easier to be bent than a

* To whom correspondence should be addressed. E-mail: zhong.zhang@nanoctr.cn, ssxie@aphy.iphy.ac.cn.
† Beijing National Laboratory of Condensed Matter, Institute of Physics, Chinese Academy of Sciences.
‡ National Center for Nanoscience and Nanotechnology.
§ Rice University.
|| State Key Laboratory of Nonlinear Mechanics (LNM), Institute of Mechanics, Chinese Academy of Sciences.
⊥ Beijing Institute of Aeronautical Materials.
Graduate School of the Chinese Academy of Sciences.

10.1021/nl901035v CCC: $40.75
Published on Web 07/08/2009

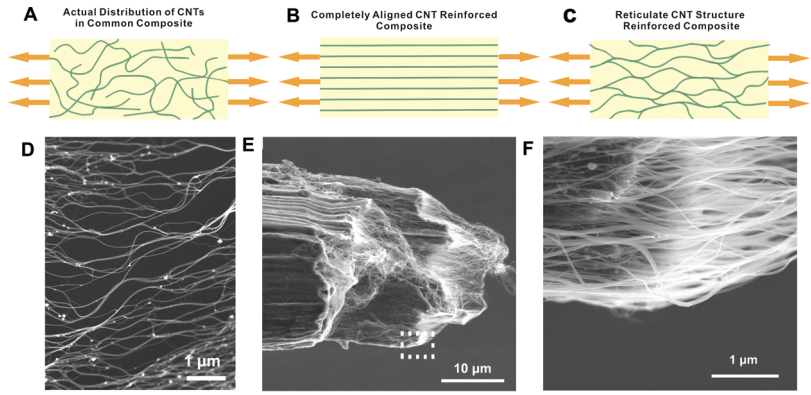

Figure 1. Hierarchical structure and morphology of CNT-reinforced composites. Schematic illustration of the internal architecture of (A) discrete CNT reinforced composite, (B) completely aligned CNT reinforced composite, and (C) r-CNT reinforced composite. (The density of the CNT is intentionally sparsely sketched to clearly demonstrate the structure.) (D) SEM image of SWNT network in a single layer. (E) Side-view SEM image of the fracture section for an epoxy-infilitrated composite fiber. Generally speaking, the fracture section shows a brittle rupture, although some SWNT bundles are pulled out by about several micrometers from the matrix. (F) Enlarged SEM image for the enclosed zone in Figure 1e. The unbroken part left looks darker due to the filling of the polymer, where the hierarchical structure of the composite can be seen.

carbon fiber with a diameter of 10 μm since the flexibility of a pillar-like structure is inversely proportional to the quartic power of its diameter. So CNTs always keep severe waviness under their natural status, which largely impairs their reinforcement effect.[8] The other is the limited interfacial shear strength between CNTs and polymer matrix. Because of CNTs' atomically smooth surfaces, their bonds to the matrix are noncovalent if no chemical modification is applied to the walls of CNTs, which results in ubiquitous interfacial slippages[9] when local stress is increased to an extent. Because of the two factors above, even if homogeneous dispersion is achieved, CNTs in composites actually carry a load much lower than they are anticipated. This gives us a sense of how much potential is actually realized in a CNT/polymer composite. As known, Raman peaks of single wall carbon nanotubes (SWNTs) down-shift to a lower wavenumber when axial strain is applied on the tubes. For PVA/PVP/SWNT composite film made by mixture,[10] 4.8 cm^{-1} peak shift of SWNT's G′ Raman band was observed per 1% strain, and the final Raman shift is 15 cm^{-1} when the composites are broken. Cronin et. al[11] observed that when 1% axial strain was applied to individual SWNTs, on average there will be an downshift of 37.5 cm^{-1} for their G′ band. The differences of Raman shifts indicate that only 13% macroscale strain of that composite comes from axial extension of SWNTs, and the SWNTs are merely stretched by 0.4% when the composites fail, although theoretically they can sustain 5.8% stain[12] before their failure.

To improve load-transfer efficiency, a great deal of efforts has been made to strengthen CNT/polymer interface by grafting functional groups.[13,14] But the attention paid to the design of load-transfer-favored structure is scarce. For other type of nanoscale building blocks such as clay or platelet-like ceramic, some successful cases of good load transfer involve the bioinspired design of nanoscale hierarchical and layered architectures facilitating the load transfer between the polymer and nanoscale building blocks,[15,16] which gives hints to CNT-based composites. Figure 1a shows the status of CNTs with optimal dispersion in composites made by mixture: short, curved, and random-oriented CNTs discretely embedded in the polymer matrix. Such distribution is obviously not conducive to transferring load onto CNTs. It has been proposed for years that if we build composites based on continuous and perfectly aligned macroscale CNTs (Figure 1B), the load will be continuously carried by strong CNTs even under moderate interface strength.[17] Vertically aligned CNT arrays are mainly closed to such reinforcing structure. But their millimeter-scale lengths disenable them from bearing tensile load,[18] and there seems to be little chance that we can obtain CNT arrays with lengths of tens of centimeters in the near future. Besides, severe delamination under such hierarchical structures is expected, just like what happened for fiber reinforced composite laminas.

Reticulate structure has its advantage on evenly delivering load over a large area. Nature has employed such structures as the veins of leaves for millions of years. If we build composites based on CNT architectures with reticulate structure, the load on the tubes could be continuously transferred though the network rather than merely through weak polymer/CNT interfaces. Besides, the waviness of the tubes could also be mitigated owning to the restriction of nearby framework. Figure 1C schematically illustrates the architecture of reticulate CNT structure-based composite. One key determing the mechanical performance of such composites is the strengths of CNT network's junctions. Right now, the postdeposited assemble of short discrete CNTs such as Bucky paper cannot meet the requirement of high strength junctions.[6] The directly synthesized macroscale CNT architectures such as fibers[19−21] and films[22,23] have their prospects. In these architectures, CNTs with moderate length are assembled as macroscale reticulate networks through strong interbundle junctions and entanglements. Take directly synthesized SWNT films as an example;[23] local stress as high as 1 GPa on the bundles could be transferred across SWNT networks through interbundle shear-lag, which results in 1 order of magnitude enhancement of tensile strength compared with Bucky paper. Up to now, there have been a few sporadic pioneer works about macroscale CNT architecture-based

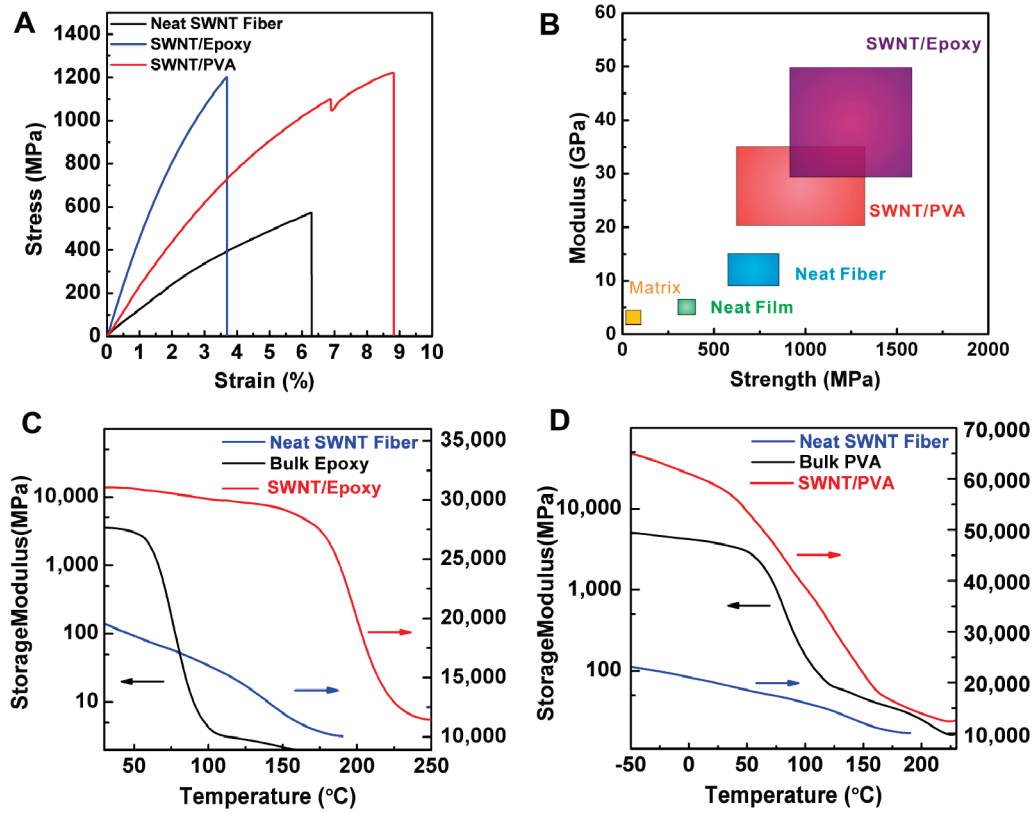

Figure 2. Mechanical properties of tested samples. (A) Typical tensile test results for composite fibers and neat SWNT fibers. The small kink on the tensile curve of PVA-infilitrated fiber indicates its robustness against defects. (B) Summary of the tensile modulus and strength for tested samples. For nonlinear tensile curves, we adopt secant modulus value at strain of 1% as tensile modulus. (C) Storage modulus for neat fiber, bulk epoxy, and composite fiber as a function of temperature. The reference bulk epoxy sample was also cured from acetone solution. (D) Storage modulus for neat fiber, bulk PVA, and composite fiber. It should be pointed out that, compared with the modulus value derived from tensile tests, the storage modulus value for PVA-infiltrated composite fiber during the glass transition is obviously inflated in the dynamic mechanical test due to its viscoelastic behavior.

composites,[20,24,25] but the study concerning reticulate CNT architecture-based composites is still in its early stage. Many fundamental issues such as what determines their mechanical properties and how continuous CNT network plays with polymer matrix have not been clearly illustrated.

In this paper, based on the results of series static and dynamic mechanical tests and Raman spectra, we first lift the veil on reticulate CNT structure (r-CNT) reinforced composites. It is found that reticulate CNT architecture not only works as continuous load-transfer pathway, but also strongly couples with polymer chains at the molecular level, which results in unique mechanical properties completely different with conventional composites. Owing to the highly efficient load-transfer in such hierarchical composites, the true potential of CNTs can be realized as initially envisioned. The synthesis of the composites is based on macroscale CVD-grown SWNT thin films. Figure 1D clearly shows the reticulate structure in the pristine films, where SWNTs have self-assembled into continuous networks through hierarchical branching of bundles. Under the assistance of CNT-affinitied solvent, high molecular weight polymer molecules were intercalated into the interspaces of CNT network without any issues with their high viscosity in liquid state. Epoxy resin and poly(vinyl alcohol) (PVA) were adopted as polymer matrices to represent typical behavior of thermoset and thermoplastic polymers respectively. Through an infiltration-twisting process, composite fibers with the length of several centimeters were fabricated for further tests (for details, see Supporting Information). The internal architecture of the composite is just like that illustrated in Figure 1C and verified by Figure 1E. By adjusting the concentration of the polymer solution, the volume fraction of SWNT was controlled in the range of 30∼50%. Under such high volume fraction, the average distance between SWNT bundles is only about 10 nm, which is even smaller than the diameters of the SWNT bundles and in the order of the lengths of polymer segments. So the SWNT network and polymer chains in fact constitute a nanoscale interpenetrating system, where strong coupling between the motions of the two components is expectable.

More than one hundred samples were tested on a tensile testing machine (Instron 5848), and their mechanical properties are summarized in Figure 2A,B. Since CNTs' volume fraction cannot be accurately controlled through infiltration method, the mechanical properties of the composite fibers show a range. The strength values for epoxy- and PVA-infiltrated fibers range from 0.9 to 1.6 GPa and 0.7 to 1.3 GPa, respectively. Compared with Bucky Paper based high-CNT-content composites, the tensile strengths of our composite fibers are more than one order higher, which means 10 times more potential of CNTs is released in r-CNT-based composites. The median strength of the epoxy-infilitrated fibers is roughly equivalent to that of continuous carbon fiber

reinforced unidirectional tapes (T300/epoxy, fiber volume of 60%)[26] even though their volume fractions of reinforcement are typically lower (30∼40%). Besides the high strength values, there are three other characterisitics that distinguish r-CNT reinforced composites from conventional composites: (1) The filling of low modulus polymers results in striking enhancement of modulus compared with neat SWNT fibers. For conventional composite materials, it is known as a common sense that the modulus of a composite must fall between that of its components. But for our r-CNT reinforced composite fibers, their moduli are much higher than that of the neat fibers and polymer matrix, which obviously goes beyond the well-known rule of mixtures. Specifically, according to the rule of mixtures the modules of epoxy- and PVA-infiltrated composite fiber should be in the range of 4−6 and 5−7 GPa, respectively, which are notably lower than the experimental values of 30−50 and 20−35 GPa. (2) The composite fibers' tensile strengths are also notably enhanced after the infiltration of low strength polymers. (3) The mechanical properties of the composite fibers strongly depend on the molecular configuration of added polymers rather than their bulk mechanical properties. For example, the modulus of bulk epoxy is not far from that of PVA, while the moduli of epoxy-infiltrated composite fibers are significantly higher than that of PVA-infilitrated fiber. These characteristics indicate r-CNT reinforced composite is completely different from conventional micrometer-sized fiber reinforced composites. Continuous CNT network and spatially confined polymer compose a nanosystem, whose performance is characterized by the molecular level coupling of the two components rather than by the rule of simple mixture. Such coupling is also reflected in the thermomechanical property of the composites. Figure 2C,D presents dynamic mechanical analysis (DMA) results of the storage modulus for neat fiber, matrix, and composite fiber as a function of temperature. The glass transitions of the polymer matrix in the composites are notably up-shifted or broadened, which unquestionably indicate the influences of SWNT network on the segmental motion of polymer chains.[27]

From the DMA results, more information about the couplings can be obtained. When composite fibers are at the temperature higher than the glass transition temperatures (T_g) of the polymer matrix, their moduli return to that of neat fibers. So it can be deduced that the couplings between polymer chains and the SWNT network does not occur when the polymers are in their rubbery state. Besides, it should be noted that the glass transition leads to an enhancement of modulus of more than 20 GPa for r-CNT/epoxy composite fibers, which is far higher (10 times) than that of the modulus of neat epoxy resin. So the enhancement should come from promoted load-bearing level of SWNTs when they are coupled with glassy polymer chains rather than from polymer matrix. In fact, only promoted load-bearing of SWNTs can give a good explanation to the one-order improvement of strengths in r-CNT based composite fibers.

To unveil the load-bearing status of the SWNTs in the composite fibers, we employ in situ Raman measurements. Figure 3a shows typical G′ band Raman spectra of the

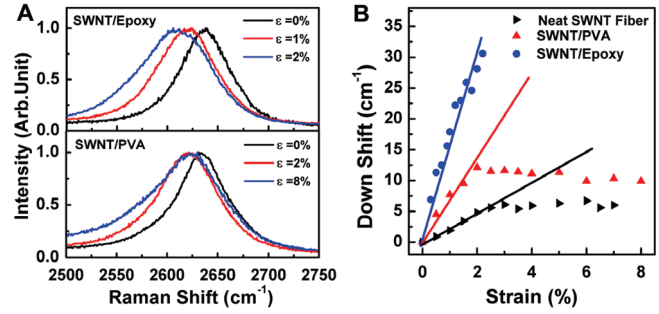

Figure 3. Variations of SWNTs' G′ band Raman spectra under strain in different systems. (A) Typical G′ band Raman spectra of epoxy or PVA-infiltrated composite fibers. (B) Downshifts of the peak position in different systems. Straight lines are plotted to guide the eyes.

composite fibers under strain. Similar to neat films and fibers,[28] the downshifting trend of the peak position and the broadening of the line shape are the major characteristics in both types of specimens. The variation of the peak positions is summarized in Figure 3B. For epoxy-infiltrated composite fibers, they have the highest downshift rate and the line shapes are symmetrically broadened with increased strain. PVA-infiltrated composite fibers show two-stage feature. At low strains, the downshifts increase linearly with strain; once the strains exceed a certain point, downshifts of G′ band plateau occurs until the final breakage of the specimens. It should be noticed that in contrast to the symmetric broadening for epoxy-infiltrated composite fiber, most broadening of the line shape for PVA-infiltrated composite fiber at large strain comes from the low wavenumber edge.

From the elevated downshift rate of G′ Raman band, it can be inferred that more macroscale strain comes from the axial extension of CNTs in composite fibers than in neat fibers, or more load is carried by CNTs at given macroscale strains from another point of view. Let us define strain transfer factor (STF) as the ratio of downshift rate for macroscale specimens to that for axially strained individual SWNTs (37.5 cm^{-1}/1% strain), which gives quantitative evaluation of how much macroscale strain comes from SWNTs' axial extension. The STF for neat fiber, PVA-, and epoxy-infiltrated composite fiber is 0.045, 0.18, and 0.4, respectively, which means there is a 4 and 9 times improvement on the strain transfer efficiency with the introduction of PVA and epoxy. For neat reticulate CNT architectures, although load can be continuously transferred and the ultimate strengths of the junctions are high, there is no way to restrict the free deformation of the CNT meshes. So macroscale strain mainly comes from the deformation of the network rather than axial extension of CNTs. The elevated SFTs for r-CNT-based composite fibers indicate that free deformations of the network are effectively "frozen" by surrounding polymer chains because of molecular level couplings, which as a result lead to higher moduli compared with neat SWNT fibers. With such a picture about the reinforcing mechanism, an explanation concerning why the moduli of the composite fibers does not rely on the bulk moduli of the matrices but their molecular configurations could be proposed. Compared with PVA, epoxy is more

Table 1. Comparison of the Predicted Modulus with Experimental Results

			Predicted modulus (GPa)[a]					
specimen type	volume fraction *(f)*	STF(α)	$\langle\cos^2\theta\rangle = 1/3$	$\langle\cos^2\theta\rangle = 0.4$	$\langle\cos^2\theta\rangle = 0.5$	$\langle\cos^2\theta\rangle = 0.6$	experimental modulus (GPa)	reference
epoxy/SWNT	0.3−0.4	0.4	27−36	32−43	40−53	48−63	30−50	this work
PVA/SWNT	0.4−0.5	0.18	17−21	19−25	24−31	29−37	20−35	this work
Neat SWNT fiber	0.65−0.75	0.045	6−7	7−9	9−11	11−13	9−15	ref 28
PVA/PVP/SWNT[b]	0.05	0.13	3.9				4.0 ± 0.2	ref 10
PVA/SWNT[b,c]	0.006	0.1	2.5				3.8 ± 0.1	ref 31

[a] The parameter of average modulus value of SWNTs (in bundle) is adopted as 640 GPa. [b] The SWNTs are discrete CNTs. [c] It seems not suitable to apply eq 2 in the cases where CNTs' volume fraction is very low. In these cases, CNTs play the role of crystalline nuclei rather than as load-carrier.

effective to block SWNT network's deformation. This is because unlike linear long PVA molecules, for epoxy resin relatively short molecules covalently cross link into an intact 3D network after it is cured. Orientation or rotation of SWNTs in such postformed 3D epoxy network is much more difficult than within the PVA matrix, so epoxy-infiltrated fibers have higher moduli at room temperature. Once polymer matrices lose their molecular holding against nanotube networks, for example, when heated above T_g (as seen in Figure 2C,D), the composites will behave like neat fibers.

On the basis of the understanding above, we can see the real load-bearing status of CNTs plays a center role in the determination of r-CNT reinforced composites' moduli. Although molecular level couplings between CNT networks and polymer matrixes may be complicated, STF, as a quantified parameter linking macroscale strain with CNTs axial tension, provides adequate information about CNTs' load-bearing status and helps us reveal the reinforcing mechanism of r-CNT based composites. For neat SWNT fibers, tubes waviness and interbundle slippage limit the load-bearing of SWNTs, so their mechanical performances are far below that of individual CNTs. After compositing with polymers, although low-modulus polymer matrixes are introduced, the strain transfer efficiencies of SWNTs are greatly enhanced owing to molecular level couplings, which lead to better mechanical properties as a result. If we view the composite fibers as composited from neat SWNT fibers and polymer matrix, as shown before, conventional composite theory that uses the rule of mixtures fails to describe the mechanical properties of r-CNT-based composites here, since CNTs' mutable load-bearing status is not involved in its theoretical framework. A successful theory that tries to describe CNT-reinforced composites should involve CNTs' load-bearing status in matrices and provide correct prediction of their mechanical properties based on micromechanical models.

With the introduction of STF, the real load-bearing status of CNTs is quantified, and we find that the modulus of r-CNT-based composite can be well described by a revised rule of mixtures. Generally, the rule of mixtures for conventional fiber reinforced composite can be expressed as[29]

$$E_c = \langle\cos^4\theta\rangle\eta_l f E_f + (1 - f)E_m \quad (1)$$

where E_c, E_f, and E_m are the Young's modulus of the composite, fibers, and matrix, respectively. f and η_l are the volume fraction and length efficiency factor of the fibers, respectively. $\langle\cos^4\theta\rangle$ describes the influence of the fibers' orientation to the modulus of the composite. η_l describes interfacial load transfer efficiency related with the aspect ratio of the fibers. For SWNT reinforced composite, if we view the reinforcements are the nanotube bundles with average modulus of 640 GPa, a problem arises for the determination of η_l in eq 1. A commonly used expression for straight fibers cannot be applied to CNTs because of their severe waviness and mutable load-bearing status. Specifically, in our case the aspect ratio of SWNTs are higher than 100, so η_l is very close to 1 according to straight-fiber model, which will give much higher prediction of the modulus than experimental observations. Besides, the differences of mechanical properties between PVA- and epoxy-infiltrated composite fibers cannot be explained in eq 1. Now with STF, a direct link between macroscale strain and CNTs' axial extension is founded, and the modified rule of mixtures could be written as (derivation in Supporting Materials)

$$E_c = \langle\cos^2\theta\rangle\alpha f E_t + (1 - f)E_m \quad (2)$$

where α is the strain transfer factor, which takes the place of η_l in eq 1 to describe the load-bearing status of CNTs in the composite, and E_t is the average modulus of single-walled carbon nanotubes (in bundles). Besides, $\langle\cos^2\theta\rangle$ replaces $\langle\cos^4\theta\rangle$ with the value of 1/3 for 3D random orientation system, since some orientation effect has been contained in STF. Theoretically, the value of $\langle\cos^2\theta\rangle$ could be obtained by averaging the orientation angles of the SWNT segments in the continuous network. But right now there is no experimental measure to determine it for our composite fibers, so here we treat it as unsettled parameter. Table 1 lists the predicted modulus given by eq 2 and the experimental results (some data from other reports are also cited for comparison). From the table, we can see that the revised rule of mixtures fits the experimental data very well with the $\langle\cos^2\theta\rangle$ value of 0.4−0.6, as in our composite fibers. If we notice that for a given CNTs' orientation, the theoretical upper limit of the STF is $\langle\cos^2\theta\rangle$, it can be inferred that the STF value for our epoxy-infilitrated composite fibers (0.4) has been very close to its upper limit and the deformation of CNT network and interbundle slippage is almost completely constrained by the chemically cross-linked epoxy network.

The molecular level couplings between r-CNT and polymer chains not only effectively constrain the free deformation of CNT networks but also greatly enhance the strength of

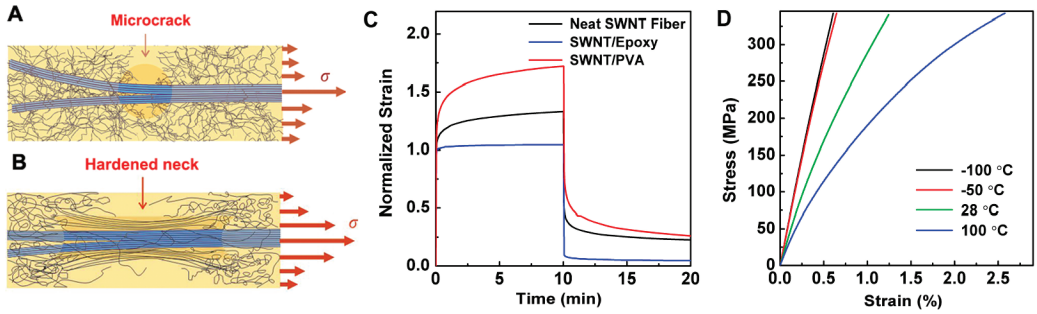

Figure 4. Fracture mechanism and viscoelastic property of r-CNT reinforced composite fibers. Schematic illustration of the fracture mechanism for (A) epoxy- and (B) PVA-infilitrated composite fiber. (C) Creep and recovery curves of composite fibers and neat fiber at initial strain of 0.5%. (D) Tensile curves for a PVA-infilitrated fiber under different temperature. To avoid fracture, the maximum stress is limited during the tensile tests.

their junctions. Take epoxy-infiltrated composite fibers as example. Their final Raman downshift reaches 31 cm^{-1}, which corresponds to real axial strain of 0.84% for the SWNTs in the matrix. Multiplying SWNT bundles' average modulus of 640 GPa,[30] there will be an average 5.4 GPa stress imposed on the SWNT bundles before the failure of the composites, which demonstrates a 5.4 times strengthening of the junctions after the filling of the low-strength epoxy. Only interactions taking place at molecular scale between r-CNT and polymer chains can give any explanation to such significant enhancements. The infiltrated polymers should not only hinder the interbundle slippages, but also mitigate the stress concentration at junctions, introduce new energy-dissipation mechanisms. Here we mainly focus on the difference of the failure process under a different type of couplings. For epoxy-infiltrated composite fibers, their failure strains are very close to that of bulk epoxy resin, and the Raman downshifts linearly increase with strain to about 31 cm^{-1} until their failure. So we have good reason to speculate the failure of epoxy-infiltrated composite results from catastrophic rupture of the SWNT network when the polymer matrix fails. In contrast to the situation of epoxy-infiltrated fibers, PVA-infiltrated composite fibers have much higher failure strains, and their Raman spectra shows a two-stage feature and asymmetric broadening, which are evidence of interbundle slippage and inhomogeneous stress distribution in the SWNT network.[28] So the fracture process for the r-CNT/PVA system is different from that of r-CNT/epoxy system. Figure 4 schematically illustrates the fracture mechanisms in the two systems. For epoxy matrix, translational movements of the molecular segments are highly constrained by the chemically cross-linked 3D network. Although such molecular rigidity significantly elevates the strain transfer efficiency, it also impairs the ductility of the SWNT network. When microcracks emerge in matrix near the junctions, the stresses at the tips of the cracks are much higher than at other places, but there is no way to dissipate the energy since free deformation of SWNT network is also constrained. So the cracks propagate very fast, and the failure strains of the epoxy-infiltrated composite fibers are very close to that of bulk epoxy resin. In contrast to epoxy, plastic flow is possible for PVA matrix with the orientation and stretching of linear PVA molecules. Under large strains, although microcracks have emerged in the PVA matrix, hardening also occurs at their tips due to the alignment of PVA molecules, which mitigate stress concentration and protect the junctions even though interbundle slippages are widespread. So the failure strains of the PVA-infiltrated composite fibers are not determined by that of the polymer matrix but the extension limit of the SWNT network. Since a great deal of mechanical energy is dissipated during the alignment of PVA molecules and the frictional sliding of the SWNT bundles, PVA-infiltrated composite fibers show apparent flaw-tolerance and higher toughness than epoxy-infiltrated fibers. Typically, the toughness of the PVA-infiltrated composite fiber could reach 50 J/g, which is far superior to most commercially used high strength fiber such as Kevlar (33 J/g) or graphite fibers (12 J/g).

A ubiquitous energy dissipation mechanism under loading is the most interesting feature of r-CNT/PVA system. At low strain, the PVA-infilitrated composite fibers show viscoelastic behavior because of the relaxation of polymeric segments, which implies their application potential as high-modulus mechanical damping materials. Figure 4c shows the creep and recovery curves at initial strain of 0.5%, where PVA-infilitrated fiber has the largest delayed elastic deformation and viscous deformation among the three types of samples. Tentatively, we can infer that PVA segments near the carbon nanotube network are easier to move under the drag of SWNTs, which results in the viscoelastic behavior and a wide relaxation time spectrum (Figure 2d). When tensile tests are performed at higher temperature (Figure 4d), segmental movements are easier, the moduli of the composite fibers drop and the nonlinear feature of the tensile curve is more remarkable. At lower temperature, since the movements of PVA segments are more strictly frozen, PVA-infilitrated fibers lost their viscoelastic feather and perform exactly like epoxy-infilitrated fiber with notably elevated modulus (~50 GPa). Such transition supports our opinion that molecular level couplings determine the mechanical properties of r-CNT based composites.

To conclude, in contrast to conventional composites, the infiltration of low-modulus and low-strength polymers does not weaken macroscale CNT fibers but further strengthens them, which goes beyond rules of mixtures. Superior mechanical properties of reticulate carbon nanotube architecture reinforced composites result from the couplings between CNT network and polymer chains occurring at

molecular level. Rigid coupling could effectively constrain the deformation of the carbon nanotube network and results in strong and stiff composites. Plastic coupling contains more segmental relaxation of the polymer and leads to higher toughness and viscoelasticity at room temperature. In epoxy/r-CNT-composite fibers, the strain transfer efficiency can approach its theoretical limit, and the final stress of 5.4 GPa carried by the SWNT bundles is also near 50% of the maximum observed strength value of 11 GPa for an isolated 20 nm diameter bundle.[3] These results show that with the combination of load-transfer-favored CNT architecture and proper molecular level couplings true potential of CNT can be realized in polymer matrix as wished.

Acknowledgment. This work is supported by National Natural Science Foundation of China (Grants 10334060, 50572119, 20874023, and 10572142), "973" National Key Basic Research Program of China (Grants 2005CB623602, 2007CB936803), the Key Item of Knowledge Innovation Project of Chinese Academy of Science (KJCX2-YW-M01), and Foundation of National Key Laboratory of Advanced Composites (9140C440201060C4401).

Supporting Information Available: S1, description of the manufacture process of the composite fibers and the used test methods. S2, derivation of the eq 2. This material is available free of charge via the Internet at http://pubs.acs.org.

References

(1) Wagner, H. D. *Nat. Nanotechnol.* **2007**, *2* (12), 742–744.
(2) Yu, M. F.; Lourie, O.; Dyer, M. J.; Moloni, K.; Kelly, T. F.; Ruoff, R. S. *Science* **2000**, *287* (5453), 637–640.
(3) Yu, M. F.; Files, B. S.; Arepalli, S.; Ruoff, R. S. *Phys. Rev. Lett.* **2000**, *84* (24), 5552–5555.
(4) Coleman, J. N.; Khan, U.; Blau, W. J.; Gun'ko, Y. K. *Carbon* **2006**, *44* (9), 1624–1652.
(5) Wang, Z.; Liang, Z. Y.; Wang, B.; Zhang, C.; Kramer, L. *Composites, Part A* **2004**, *35* (10), 1225–1232.
(6) Gou, J. H. *Polym. Int.* **2006**, *55* (11), 1283–1288.
(7) Coleman, J. N.; Blau, W. J.; Dalton, A. B.; Munoz, E.; Collins, S.; Kim, B. G.; Razal, J.; Selvidge, M.; Vieiro, G.; Baughman, R. H. *Appl. Phys. Lett.* **2003**, *82* (11), 1682–1684.
(8) Fisher, F. T.; Bradshaw, R. D.; Brinson, L. C. *Compos. Sci. Technol.* **2003**, *63* (11), 1689–1703.
(9) Ajayan, P. M.; Tour, J. M. *Nature* **2007**, *447* (7148), 1066–1068.
(10) Zhang, X. F.; Liu, T.; Sreekumar, T. V.; Kumar, S.; Moore, V. C.; Hauge, R. H.; Smalley, R. E. *Nano Lett.* **2003**, *3* (9), 1285–1288.
(11) Cronin, S. B.; Swan, A. K.; Unlu, M. S.; Goldberg, B. B.; Dresselhaus, M. S.; Tinkham, M. *Phys. Rev. Lett.* **2004**, *93* (16), 4.
(12) Walters, D. A.; Ericson, L. M.; Casavant, M. J.; Liu, J.; Colbert, D. T.; Smith, K. A.; Smalley, R. E. *Appl. Phys. Lett.* **1999**, *74* (25), 3803–3805.
(13) Hwang, G. L.; Shieh, Y. T.; Hwang, K. C. *Adv. Funct. Mater.* **2004**, *14* (5), 487–491.
(14) Blake, R.; Gun'ko, Y. K.; Coleman, J.; Cadek, M.; Fonseca, A.; Nagy, J. B.; Blau, W. J. *J. Am. Chem. Soc.* **2004**, *126* (33), 10226–10227.
(15) Podsiadlo, P.; Kaushik, A. K.; Arruda, E. M.; Waas, A. M.; Shim, B. S.; Xu, J. D.; Nandivada, H.; Pumplin, B. G.; Lahann, J.; Ramamoorthy, A.; Kotov, N. A. *Science* **2007**, *318* (5847), 80–83.
(16) Bonderer, L. J.; Studart, A. R.; Gauckler, L. J. *Science* **2008**, *319* (5866), 1069–1073.
(17) Chae, H. G.; Kumar, S. *Science* **2008**, *319* (5865), 908–909.
(18) Ci, L.; Suhr, J.; Pushparaj, V.; Zhang, X.; Ajayan, P. M. *Nano Lett.* **2008**, *8* (9), 2762–2766.
(19) Li, Y. L.; Kinloch, I. A.; Windle, A. H. *Science* **2004**, *304* (5668), 276–278.
(20) Baughman, R. H.; Zhang, M.; Atkinson, K. R. *Science* **2004**, *306* (5700), 1358–1361.
(21) Koziol, K.; Vilatela, J.; Moisala, A.; Motta, M.; Cunniff, P.; Sennett, M.; Windle, A. *Science* **2007**, *318* (5858), 1892–1895.
(22) Baughman, R. H.; Zhang, M.; Fang, S. L.; Zakhidov, A. A.; Lee, S. B.; Aliev, A. E.; Williams, C. D.; Atkinson, K. R. *Science* **2005**, *309* (5738), 1215–1219.
(23) Ma, W. J.; Song, L.; Yang, R.; Zhang, T. H.; Zhao, Y. C.; Sun, L. F.; Ren, Y.; Liu, D. F.; Liu, L. F.; Shen, J.; Zhang, Z. X.; Xiang, Y. J.; Zhou, W. Y.; Xie, S. S. *Nano Lett.* **2007**, *7* (8), 2307–2311.
(24) Li, F.; Cheng, H. M.; Bai, S.; Su, G.; Dresselhaus, M. S. *Appl. Phys. Lett.* **2000**, *77* (20), 3161–3163.
(25) Bogdanovich, A.; Bradford, P.; Mungalov, D.; Fang, S. L.; Zhang, M.; Baughman, R. H.; Hudson, S. *SAMPE J.* **2007**, *43* (1), 6–19.
(26) *Composite Materials Handbook- MIL 17*; Department of Defense: Washington, DC, 2002; Vol. 2.
(27) For SWNT/ PVA composites, the environments for PVA molecule segments are not uniform under the influence of surrounding CNTs, which results in the broadened glass transition. Such phenomenon was also observed by other researchers (Miaudet, P.; Derre, A.; Maugey, M.; Zakri, C.; Piccione, P. M.; Inoubli, R.; Poulin, P. *Science* 2007, *318*, (5854), 1294−1296). For the SWNT/epoxy composite fibers, the up-shift of the T_g looks unbelievably large (over 100°C), and this may be related with added acetone in the reference bulk epoxy. Considering SWNT networks were infiltrated by epoxy/acetone solution, for reasonable comparisons the reference bulk epoxy in Figure 2c was also cured from acetone solution, which largely decreases its T_g. In fact, the T_g for the used pure epoxy without acetone is 160 ∼ 170 °C. So compared with the epoxy without acetone, the T_g up-shift of CNT/epoxy composite fiber is about 10 ∼ 20 °C.
(28) Ma, W. J. *Adv. Mater.* **2009**, *21*, 603–608.
(29) Krenchel, H. *Fibre reinforcement*; Akademisk Forlag: Copenhagen, 1964.
(30) Gao, G. H.; Cagin, T.; Goddard, W. A. *Nanotechnology* **1998**, *9* (3), 184–191.
(31) Liu, L. Q.; Barber, A. H.; Nuriel, S.; Wagner, H. D. *Adv. Funct. Mater.* **2005**, *15* (6), 975–980.

NL901035V